

Evaluating an Accelerometer-based System for Spine Shape Monitoring

Katharina Stollenwerk¹, Johannes Müllers², Jonas Müller²,
André Hinkenjann¹, and Björn Krüger²

¹ Hochschule Bonn-Rhein Sieg, Institute of Visual Computing, Sankt Augustin,
Germany

² Gokhale Method Institute, Stanford CA, United States

Abstract In western societies a huge percentage of the population suffers from some kind of back pain at least once in their life. There are several approaches addressing back pain by postural modifications. Postural training and activity can be tracked by various wearable devices most of which are based on accelerometers. We present research on the accuracy of accelerometer-based posture measurements. To this end, we took simultaneous recordings using an optical motion capture system and a system consisting of five accelerometers in three different settings: On a test robot, in a template, and on actual human backs. We compare the accelerometer-based spine curve reconstruction against the motion capture data. Results show that tilt values from the accelerometers are captured highly accurate, and the spine curve reconstruction works well.

1 Introduction

Lower back pain is one of the largest diseases in the United States. In fact, 31 million Americans experience lower back pain at any given time [1]. Thus, lower back pain is the single leading cause of disability worldwide, according to the Global Burden of Disease 2010. Back pain is one of the most common reasons for missed work. In fact, back pain is the second most common reason for visits to the doctor's office, outnumbered only by upper-respiratory infections. One-half of all working Americans admit to having back pain symptoms each year [2]. Experts estimate that as much as 80% of the population will experience a back problem at some time in their lives [3], and that back pain is the largest single factor in the economical costs of \$560-\$635 billion per year attributed to pain in the United States [4].

There is a wide variety of interventions. Starting from invasive methods, like spinal fusion surgery, and laminectomy (decompression) surgery, over medications like cortisone injection, oral corticosteroids, or acetaminophen, to education on posture, such as yoga, physical therapy, or postural modifications. According to the crowd-sourcing platform *HealthOutcome*¹, postural modifications are the highest rated interventions [5]. Capturing and analysing motion data through training has become a standard procedure: Gait labs using motion

¹ www.healthoutcome.org

capture setups, force plates, and other sensor technology are common. However, lab situations are not the best environment to capture and analyse a patient’s natural behaviour. Thus, with emerging sensor technology, wearable devices were included into training, bringing data capturing out of the lab. So far, studies report varying results on the effectiveness of wearable devices for postural training and monitoring: The authors of [6] found that using the *UpRight*² device leads to positive increases in awareness of posture, emotional well-being, and decreases in pain symptoms. While the authors of a study based on the *Lumo Lift*³ device, conclude [7]: “This study indicates that Lumo Lift is not suitable of giving posture feedback during lifting in daily life”. The above mentioned studies directly focus on the impact on the user, without analysing the accuracy of the sensor systems they use. Fathi and Curran [8] use three inertial sensors, distributed over the lumbar and thoracic spine, to capture body poses. They focus on classification of various postures without assessing the quality of the captured data. Thus, we focus on the accuracy of capturing posture in this work. Only if postural features are monitored accurately, devices will be able to provide valuable data that can be enhanced to give useful feedback to the user.

The remainder of this paper is organised as follows: Section 2 gives an overview of the work related to motion capturing with various sensor systems. The used sensor technology is described in Section 3. Section 4 explains how tilt angles and positional data are computed from the used accelerometers. Our recording setup and the dataset that our experiments are based on are described in Section 5. An evaluation and the underlying measures are presented in Section 6. We discuss limitations in Section 7 and conclude the paper in Section 8.

2 Related Work

Recording and analysing human motions is well established in a wide variety of domains, such as computer animation, sport sciences [9], biology [10], and rehabilitation [11]. Optical motion capturing using passive markers and a large array of cameras has become the gold standard of capturing motions due to its high temporal and spatial resolution and accuracy [12]. This recording technique allowed the development of many enhanced applications analysing human [13,14] and animal [15,16] motions. Large databases of motion data are freely available [17,18] and a variety of techniques to handle the increasing amounts of available data have been developed [19,20,21,22]. To overcome the disadvantages of complex hardware settings (number of cameras, 42 and more markers need to be attached for full body capturing), the computer vision community is developing many approaches to compute 3D reconstructions of human poses without markers from single images of video sequences [23,24]. One orthogonal approach records motions based on the data from body-mounted cameras [25,26].

The development of other sensor technologies allows for capturing without cameras, and thus without the restrictions of a capturing volume. Therefore,

² www.uprightpose.com

³ www.lumobodytech.com

wireless EMG sensors and accelerometers have become popular and are used for motion analysis [27,28,29].

Based on readings from accelerometers only, various techniques have been developed to reconstruct [30,31,32,33] and classify [8,13,34] human poses and motions. While the above mentioned methods are able to roughly reconstruct full body motions on the basis of data from five three-axis sensors, in this work we focus on an accurate reconstruction of only a part of the human body, namely the curvature of the spine at the lower back.

3 Hardware

In this section we introduce the hardware employed in our recordings. We first give a brief overview of the motion capture system. Subsequently we provide more detailed information on the accelerometer-based system.

3.1 Motion Capture System

For the recordings, we used a ten-camera OptiTrack⁴ Flex 3 system. The cameras operate at a resolution of 640×480 pixels. Throughout the recordings the frame rate was set to 100 Hz. Passive, spherical, retro-reflective markers with a diameter of 7/16 in (≈ 11 mm) were used. As output from the motion capture system we received 3D marker trajectories, which needed further cleaning and labeling. See Section 5.2 for details on these processes.

3.2 Wearable

The wearable device used in the scope of this work is the *PostureSensei*TM (see Figure 1) developed by Gokhale Method Enterprises⁵. While most posture wearables include one device, this system consists of five individual sensor units that are attached to the lower back of the user. With this approach it is possible to capture more detailed data on a larger part of the spine. Compared to readings from a single location on the body, several curvatures can be measured at once. Although a five-sensor configuration has been used, the system is in principle scalable to more or fewer sensors.

The five sensor units are technically identical and contain a three-axis accelerometer, a Bluetooth LE (low energy) module and a lithium battery. All sensors connect to one host (may be an iOS device or a computer) and stay in an energy-saving state until the measurement is started. Sampling rates of 10 Hz, 25 Hz and 50 Hz can be configured from the host, suitable for slow motion measurements like sitting, as well as faster movements such as brisk walking [30]. At 50 Hz sampling rate, a battery runtime of eight hours allows a full work day of experimenting, while 10 Hz allow posture tracking for more than 24 h.

⁴ <http://optitrack.com/>

⁵ <http://posturesensei.com>



Figure 1. Photos of the *PostureSensei™* sensor system. Four of five sensors are sitting in the charger. A single sensor has the dimensions 33 mm × 16 mm × 10 mm and is attached to a person’s back with double sided tape. The right images shows a sensor’s local coordinate system.

With a programmable full-scale-range of ± 2 g (up to ± 16 g)⁶ and 10 bit resolution, a sensitivity of ± 4 mg/LSB is achieved.

Keeping in mind that the wearables are used to reconstruct static postures due to their orientation in space, and not the actual acceleration during the movement, we shortly discuss the resulting angular resolution. To this end, it is assumed that all postures are evaluated at rest and dominated by the earth’s gravitational force. Hence the resulting force on all axes equals

$$\sqrt{a_x^2 + a_y^2 + a_z^2} = 1 \text{ g.} \quad (1)$$

In this situation, an angular resolution of roughly 0.2° is achieved. This has proven to be sufficient for all conducted measurements.

Although being very versatile for motion tracking, one has to keep in mind that with a three-axis accelerometer, rotational movements around the sensor axis pointing to the earth’s centre of gravity can not be tracked.

4 Pose reconstruction

In this section we give an overview of how we reconstruct a curve as representation for the spine shape from the accelerometers’ data. First, we estimate the orientation of each sensor. The orientations from all sensors are fed into a simple model that is the basis of the spinal curve we display.

4.1 Sensor Orientation Estimation

Assuming the sensor is not moving, which is reasonable for static poses, the sensor only measures acceleration due to gravity pointing downwards. In this case the sensor’s *forward tilt* t_{acc} is defined as follows:

$$t_{\text{acc}} = \arctan 2(a_z, -a_y) \quad (2)$$

Here, a_z denotes the measured acceleration in the sensor’s local z -axis, while a_y is the acceleration in the sensor’s local y -axis, as defined in Figure 1.

⁶ $g \approx 9.81 \text{ m/s}^2$ is earth’s standard acceleration due to gravity.

4.2 Spine Curve Computation

The spine curve is computed based on the sensor orientations. We restrict this curve to 2D to give an easy-to-understand feedback on the user's current posture.

Attaching the sensors to a person's back with the help of an applicator, the distance between each neighbouring pair of sensors is equal. Thus, we assume equal distance in our model, too. The actual spine curve consists of two components: The first component is a line representing the forward tilt of the first (lowest) sensor. The second component consists of a series of arc segments between pairs of neighbouring sensors. The number of arc segments totals four.

The arc segments between two sensors' positions P_n and P_{n+1} is computed as follows: The tilt at the beginning and the end of the arc segments is defined by the sensor's forward tilts $t_{acc,n}$ and $t_{acc,n+1}$. The included angle δ_n is the difference between these two tilts: $\delta_n = t_{acc,n} - t_{acc,n+1}$. The distance d between the points is fixed and constant between all points in our model. From these values, the arc is already completely defined. The radius r of the underlying circle is defined as:

$$r_n = \frac{d}{|\delta_n|} \quad (3)$$

The center C_n of the circle underlying the n th arc can be computed by:

$$C_n = P_n - r_n \cdot \begin{pmatrix} \cos(t_{acc,n}) \\ -\sin(t_{acc,n}) \end{pmatrix} \quad (4)$$

The end point P_{n+1} of the arc is computed by:

$$P_{n+1} = C_n + r_n \cdot \begin{pmatrix} \cos(t_{acc,n+1}) \\ -\sin(t_{acc,n+1}) \end{pmatrix} \quad (5)$$

In case the angle is less than the inherent sensor accuracy $\Delta\delta_n \approx 0.3^\circ$ a line is drawn instead of an arc segment, $\Delta\delta_n = \sqrt{(\Delta t_{acc,n})^2 + (\Delta t_{acc,n+1})^2}$. *PostureSensei™* comes with an app for data visualisation. Some examples of the reconstructed spine curves can be found in Figure 2.

5 Recording Setup and Datasets

We recorded three different scenarios (robot data, template data, human posture data) with the *PostureSensei™* sensors (at 50 Hz) and the OptiTrack system (at 100 Hz). In order to spatially track the sensors, reflective markers were attached to the sensors. These were either single spherical reflective markers or groups of four markers attached to a rigid body. The exact type and location of the markers depended on the scenario. In combination, the recorded data consists of the 3D positions of each marker or rigid body and the accelerometer data of each sensor as well as the orientation of the rigid bodies in space (4D quaternion), where applicable. The recorded datasets along with the marker setups are described in more detail in the sections below and are illustrated in Figure 3.

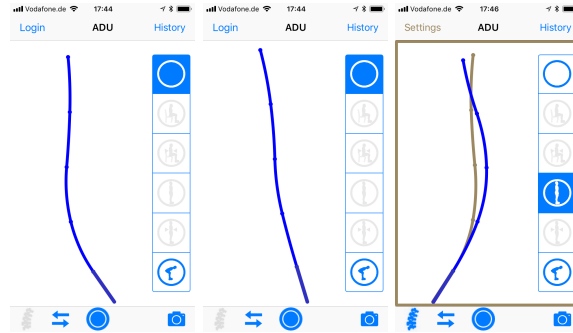


Figure 2. Screenshots from *PostureSensei*TM app of some reconstructed spine curvatures, showing various shapes. A comparison of two curves is shown in the right image.

5.1 Datasets

Robot To test if the motion sensors correctly capture their orientation, we devised some tests and mounted them vertically onto a rotatable robot arm (see Figure 3a). We used a Lego Mindstorms robot from the EV3 series. In order to track the robot arm’s orientation in space, four markers were attached approximately equidistantly (13.5 cm apart from each other) to the robot arm.

We recorded two different scenarios: R380P10 and R360P10. **R380P10** consists of a 380° clockwise rotation of the motor attached to the robot arm followed by a ten-second pause. These steps are repeated 24 times. In **R360P10** the motor rotates by 360° clockwise and pauses ten seconds three consecutive times. The rotation is executed at an average of 60° s^{-1} . The ‘average’ arises from the motor driving the arm accelerating at the beginning of each rotation and decelerating to a stop at the end of each rotation.

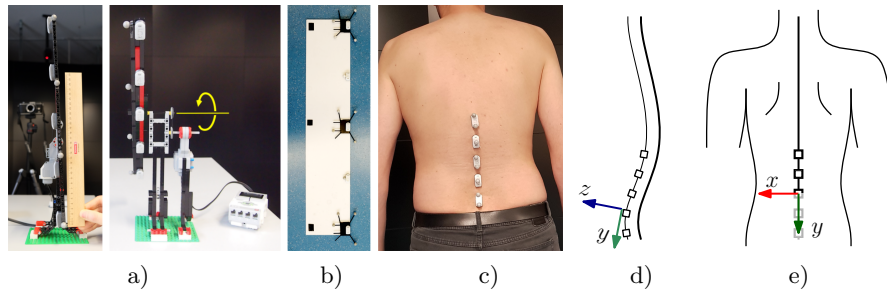


Figure 3. Photos of the recording setups: a) Sensors and markers mounted on the robot. b) Sensors, markers, and rigid body assets on the synthetic template. c) Sensors on the lumbar spine of a person. d) and e) Side and back view of sensor positioning on the lumbar spine (thick line) including directions of the sensor coordinate system.

Template Here, the sensors were placed onto a 2.5 mm strong flexible PVC foam board (template, see Figure 3b). With the sensors on the template, the template was bent stronger than usually possible for the human back.

In this scenario, rigid bodies with four spherical reflective markers each, so-called rigid body assets, were attached to three of the sensors. A single reflective spherical marker was glued to both of the remaining sensors.

Human Posture Finally, we recorded trials with the sensors attached to a person’s back as shown in Figure 3c. We only considered static standing poses. In order to spatially track the sensors, a single reflective spherical marker was attached to the centre of every sensor.

5.2 Data Preprocessing

The recorded optical motion capture data was cleaned and temporally aligned with the accelerometer data before further processing. *Data cleaning* here refers to the semi-automatic removal of inconsistent marker data and to the consistent combination of marker data from different markers. The latter is necessary when tracking individual markers. If the tracking system loses a marker, e.g. from occlusion, it will treat it like a new marker as soon as it is no longer occluded (it does not ‘know’ that it just met an old friend).

In order to compare the positional data recorded with the tracking system and the tilt data t_{acc} derived from the accelerometer data, we also compute tilt angles from the tracking data. In case of rigid body tracking, the tilt t_{opt} can be directly inferred from the recorded rotation data. In the robot arm scenarios we treat the robot arm as a rigid body represented by the markers attached to it (see limitations in Section 7). The tilt t_{opt} of the arm is computed with respect to the tracking system’s up-vector \mathbf{u} as the angle between \mathbf{u} and the robot arm. The robot arm is represented by an (oriented) line \mathbf{m} . With $\langle \mathbf{v}, \mathbf{w} \rangle$ denoting the dot product,

$$t_{\text{opt}} = \arccos \left(\left\langle \mathbf{u}, \frac{\mathbf{m}}{\|\mathbf{m}\|} \right\rangle \right). \quad (6)$$

Other processing steps before actually comparing data from the different sources are *filtering* and *downsampling* of the OptiTrack data by a factor of two, effectively reducing the sampling rate to match the 50 Hz of the *Posture-Sensei™* data. For *filtering* we use a 220 ms- to 340 ms-windowed median filter (spanning 11 to 17 samples at 50 Hz) followed by a moving average filter of the same width. This removes noise from both signals. If not otherwise stated we work with the filtered data sampled at (or downsampled to) 50 Hz.

6 Results

We recorded datasets covering a variety of poses and motions that call for different evaluation strategies depending on the respective data. These strategies will be explained in more detail in Section 6.1. Results and their discussion can be found in Section 6.2.

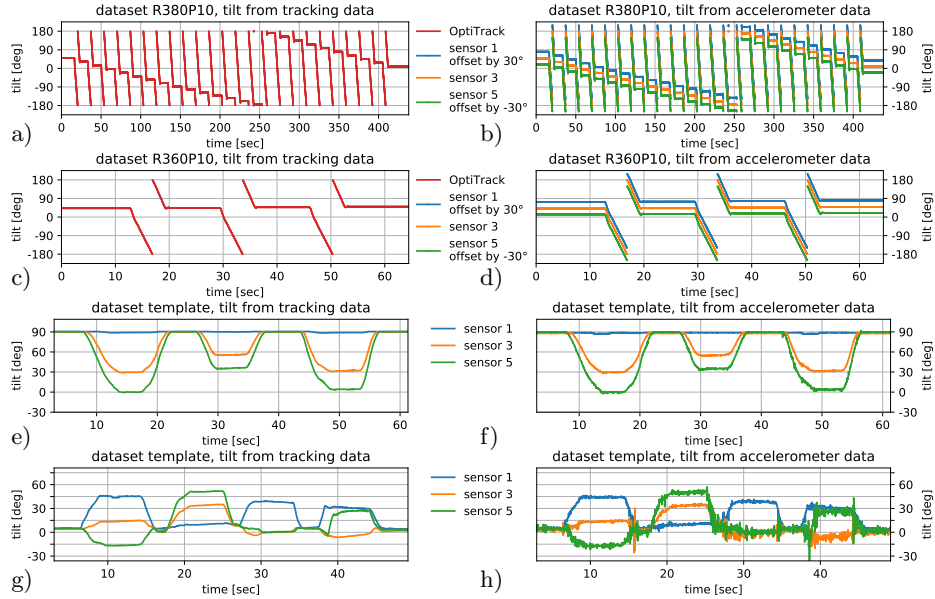


Figure 4. Computed raw tilt values for four recordings of three scenarios. Data from the OptiTrack system are shown in the left column, data from the *PostureSensei*TM are shown in the right column.

6.1 Evaluation Strategy

Dataset Robot, R380P10 For the R380P10 dataset, we will evaluate how well the tilt computed for both systems (t_{acc} for accelerometer data and t_{opt} for tracking data) compares to one another. The data recorded in this setup, especially in the raw accelerometer data and hence the derived tilt data (see first row of Figure 4), exhibit strong fluctuations every time the robot stops. We therefore, and because the arm oscillates for some seconds after stopping, extract the first five of the last six seconds of each step detected by both systems and compute the mean and standard deviation for each step as well as the overall mean step size (see Table 1). We furthermore compute the difference $t_{opt} - t_{acc}$ for each segment and sensor.

Dataset Robot, R360P10 This dataset was recorded in order to measure the consistency of t_{acc} and t_{opt} while moving. To this end, we divide the recorded data into parts with positive, zero, and negative gradient and analyse the non-constant segments.

In order to separate the tilt data into segments of equally signed gradients, we compute the gradient ∇f of the (filtered) tilt data f and apply a moving average with a fixed window width (of 340 ms) to ∇f . Using a threshold $T = 0.5^\circ$, the tilt data is divided into segments of positive ($\nabla f > T$), negative ($\nabla f < -T$),

and zero ($|\nabla f| \leq T$) gradient. Due to clockwise rotation, R360P10 only exhibits segments with zero and negative gradient (see second row of Figure 4).

We compute the Pearson correlation coefficient for each found segment with negative gradient (Figure 6 left). The Pearson correlation coefficient measures how much two signals are linearly related (e.g. by a constant offset):

$$r_{x,y} = \frac{\sum_{i=1}^n (x_i - \mu_x)(y_i - \mu_y)}{\sqrt{\sum_{i=1}^n (x_i - \mu_x)^2} \sqrt{\sum_{i=1}^n (y_i - \mu_y)^2}} \quad (7)$$

where μ_x and μ_y are the mean of x and y and $r_{x,y} \in [-1, 1]$. $r_{x,y} = \pm 1$ represents a complete positive/negative linear correlation. A value of 0 signifies that x and y are not linearly correlated.

In order to gain insight of the magnitude of a potential offset between t_{opt} and t_{acc} we compute their difference $t_{\text{opt}} - t_{\text{acc}}$.

Dataset Template In the evaluation of the template dataset, we proceed in analogy to the evaluation of R360P10, but analyse each recording as a whole (see third row of Figure 4 for raw tilt values). I.e. we compute the Pearson correlation coefficient and the median, mean, and standard deviation, as well as the absolute value of the tilt difference described above. The data is not split into gradient-segments. Evaluations were carried out on a per-sensor basis.

Dataset Human Posture For the human posture dataset, we computed a 2D spine curve from the accelerometer data as described in Section 4.2 for all frames. All frames are leveraged to 3D. As a consequence, each sensor is represented by a single 3D position. The recorded tracking dataset represents each sensor as a single 3D position by setup design. In order to measure distances in the two datasets we interpret each of them as ordered point clouds in space, P_{opt} and P_{acc} , both ordered by sensor and frame number. Each of the two point clouds can be linearly transformed to best correspond to the other point cloud. We use a Procrustes algorithm [35] to find the best fit of the two datasets. The best-fit criterion is the minimum sum of squared distances of one point cloud P_{opt} to a scaled, translated, and rotated version P'_{acc} of the other point cloud P_{acc} . We use P_{opt} as the reference dataset because P_{acc} contains unit-less data and P_{opt} is measured in metric units of length.

The quality evaluation of the computed 2D curve data compared to the 3D positions from the tracking data is performed on the aligned raw datasets P_{opt} and P'_{acc} . To this end we first draw n random samples and extract a window of ± 100 ms width around identical frames within both datasets (10 frames each at 50 Hz). For a dataset of length l , $n = l/5$ random samples suffice to consider each single frame on average twice. We then compute the point-wise Euclidean distance of each corresponding pair of points in the two datasets within the extracted window as well as their mean and standard deviation. These state how well the best match of the two point clouds was. The distances and derived quantities are measured in millimetres (see Table 4).

Table 1. Dataset R380P10. Means (μ) and standard deviations (σ) in degree for each detected step in the recorded robot data. The programmed rotation of the motor is denoted by a_α . For better readability we list only every fifth step.

sensor ID	data	μ	σ	μ	σ	μ	σ	μ	σ	μ	σ
		a_0		a_{-100}		a_{-200}		a_{-300}		a_{-400}	
	t_{opt}	0.9	0.00	-82.6	0.01	-155.5	0.01	-240.9	0.00	-329.8	0.02
1	t_{acc}	-0.0	0.08	-82.4	0.07	-153.5	0.07	-242.4	0.07	-329.8	0.03
2	t_{acc}	0.0	0.12	-82.4	0.05	-155.5	0.07	-241.6	0.05	-330.7	0.06
3	t_{acc}	0.1	0.11	-82.9	0.07	-156.7	0.06	-241.1	0.07	-331.6	0.07
4	t_{acc}	0.9	0.03	-82.9	0.03	-157.3	0.06	-240.9	0.04	-330.6	0.06
5	t_{acc}	1.1	0.08	-82.3	0.08	-156.0	0.07	-240.8	0.03	-329.8	0.06

6.2 Results and Discussion

Dataset Robot, R380P10 Table 1 summarises the average tilt computed from the acceleration sensors and from the tracking data in between each revolution of the robot arm, which are in very good agreement to each other (constant mean value and low standard deviations). The angles computed from neither the OptiTrack data nor the *PostureSensei*TM data match the step angle of -380° programmed into the robot. As the overall mean offset between programmed rotation and measured rotation lies around 3.4° , an average deviation of 1.61° per -180° programmed rotation, the robot system can't be used as a third system to compare to (see limitations in Section 7).

We computed how much the tilt angles from OptiTrack and *PostureSensei*TM differ by computing the difference $t_{\text{opt}} - t_{\text{acc}}$ as shown in Figure 5. Angle differences mostly lie within $[-1^\circ, +1.6^\circ]$. Only *PostureSensei*TM sensor 1 deviates slightly more from the OptiTrack data (by up to -3°) during seconds 100 to 180. Reasons for this behaviour may include, that the robot arm is not a rigid body (see limitations in Section 7). Nevertheless, the overall difference between the two systems $t_{\text{opt}} - t_{\text{acc}} = 0.4^\circ \pm 0.8^\circ$ is statistically equal to zero.

Dataset Robot, R360P10 In the second part of the robot dataset, R360P10, we compared non-constant segments of the data using the Pearson correlation coefficient. Results are depicted in Figure 6 (left). The data decomposes into three non-constant segments. These are the segments in Figure 4c when delet-

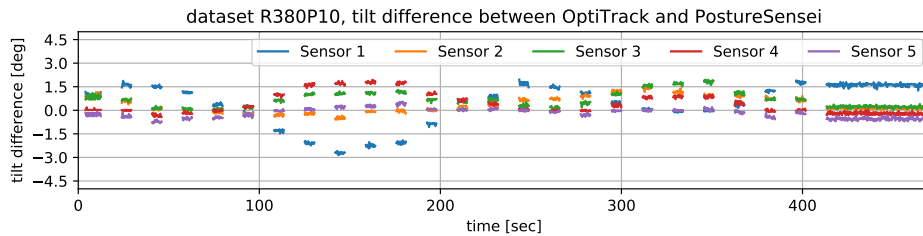


Figure 5. Difference of t_{opt} and t_{acc} for each sensor of the *PostureSensei*TM system restricted to segments with zero gradient.

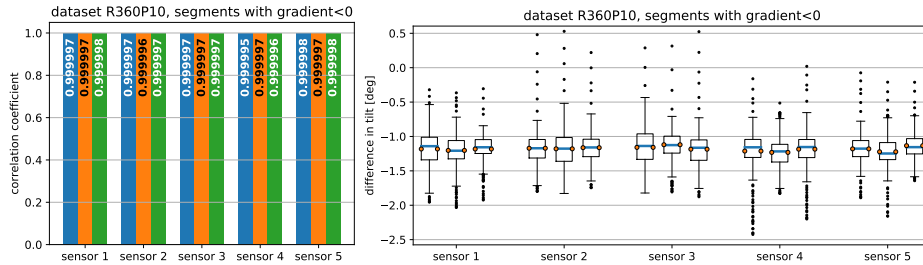


Figure 6. Left: Pearson correlation coefficient of data segments with negative gradient of R360P10-dataset. Right: Boxplot of the difference of tilt $t_{opt} - t_{acc}$ of all such segments. Mean values are indicated by the small circles on the sides of each box, the median is drawn as blue lines. Bars and boxes are grouped by sensor and sorted by time of occurrence in the data. We used a standard boxplot as provided by matplotlib⁸.

ing the constant segments. The correlation coefficient is extremely high for all segments and all sensors (minimum of 0.999995).

In addition to median and mean of the absolute difference of the accelerometer-based tilt data and the tracking-based tilt data, the boxplot on the right in Figure 6 depicts the distribution of the data. This reveals that even if the two tilt data series are highly correlated, their difference can still exhibit absolute fluctuations of up to almost 2.5° . It also shows that the difference is centred around -1.25° with respect to both, median and mean. Furthermore, the difference of over half of the data is below 1.25° . More than 75% of the differences are below 1.4° . Overall, the high similarity in shape – location of mean and median (all almost centred) as well as size of the boxplots – suggests that the differences are similarly distributed. This in turn implies a high level of consistency between the data recorded with OptiTrack and the *PostureSensei*TM sensors.

Dataset Template The template dataset was compared trial-wise as a whole using the Pearson correlation coefficient as well as median, mean, and standard deviation of the absolute difference of the tilt computed from tracking data and from accelerometer data. For this dataset, we evaluated filtered and unfiltered data. Table 2 lists the result of the correlation coefficient. Again, the correlation coefficient is very high for all trials and for most sensors. In the first four takes, the lower part of the template, containing sensor 1, was fixated to a flat surface, and the template was gradually bent by lifting its upper side until it reached an angle of approximately 90° . Therefore sensor 1 moves only minimally (see Figure 4e and f), which explains the correlation coefficient of ≈ 0.5 as the data is dominated by noise. For the rest of the takes and sensors the correlation coefficient of both data types recorded indicates that there is a very strong (positive) linear relationship between the two tilt data series (filtered data minimum of 0.998, raw data minimum 0.957).

⁸ https://matplotlib.org/api/_as_gen/matplotlib.pyplot.boxplot.html

Table 2. Dataset template, all takes. Values of Pearson correlation coefficient grouped by used data type. Left side: filtered data, right side: unfiltered, raw data.

take	sensor														
	1	3	5		1	3	5		1	3	5		1	3	5
t ₁ f	0.592	1.000	1.000	t ₅ f	1.000	0.998	0.999	t ₁ r	0.475	1.000	1.000	t ₅ r	0.991	0.957	0.992
t ₂ f	0.587	1.000	1.000	t ₆ f	1.000	0.999	0.999	t ₂ r	0.485	0.999	1.000	t ₆ r	0.995	0.988	0.993
t ₃ f	0.587	1.000	1.000	t ₇ f	0.999	0.998	0.999	t ₃ r	0.542	1.000	1.000	t ₇ r	0.991	0.975	0.984
t ₄ f	0.537	1.000	1.000	t ₈ f	1.000	0.999	0.999	t ₄ r	0.364	0.999	1.000	t ₈ r	0.996	0.979	0.987

The computation of several statistical measures, such as median, mean, and standard deviation of the difference of the two tilt data series aimed at putting that linear relation better into context (see Table 3). From the table we can see that there is only slight variation in the average absolute difference of the two data series. Deviations range from $m = 0.1^\circ$, $\mu = 0.1^\circ$, and $\sigma = 0.1^\circ$ (filtered data, take 6 sensor 1) to $m = 2.0^\circ$, $\mu = 1.7^\circ$, and $\sigma = 0.6^\circ$ (filtered data, take 4 sensor 5). These values are equally low for raw data.

Because the overall mean of the absolute difference between the two data series is a relatively abstract description of the underlying, absolute per-sample difference, we also plotted a pair of data series together with their absolute difference in Figure 7. For better readability we only included data from a single sensor. The depicted absolute difference exhibits a throughout slightly higher value when the tilt data exceeds 90° (e.g. seconds 1 to 10 and around second 25). This observed recurring difference could be attributed to minor tracking inconsistencies in the motion capturing in this range: When a registered rigid body asset is rotated close to 90° in direction of the tracking system’s up-vector, the rotation computed by the tracking system tends to jitter around 90° . Peaks also occur shortly before and after constant segments. A likely cause for these is the fact that the data is not perfectly temporally aligned. Hence directional changes in the trajectory lead to higher errors in the two signals’ difference.

Dataset Human Posture For the last dataset, we evaluate how well the computed 2D spine curve matches the 3D tracking data by measuring mean

Table 3. Dataset template, all takes. Median (m), means (μ), and standard deviations (σ) (all in degree) of absolute difference of tilt from tracking data and tilt from accelerometer data ($|t_{\text{opt}} - t_{\text{acc}}|$). Left side: filtered data, right side: unfiltered, raw data.

take	sensor 1			sensor 3			sensor 5			take	sensor 1			sensor 3			sensor 5		
	m	μ	σ	m	μ	σ	m	μ	σ		m	μ	σ	m	μ	σ	m	μ	σ
t ₁ f	1.3	1.1	0.7	1.3	1.4	0.3	1.6	1.7	0.4	t ₁ r	1.5	1.3	0.8	1.3	1.3	0.2	1.3	1.5	0.5
t ₂ f	1.2	1.0	0.6	1.2	1.3	0.3	1.5	1.6	0.5	t ₂ r	1.3	1.1	0.7	1.3	1.4	0.3	1.6	1.6	0.5
t ₃ f	1.3	1.2	0.8	1.5	1.4	0.4	1.9	1.7	0.5	t ₃ r	1.2	1.2	0.8	1.4	1.3	0.5	1.6	1.6	0.6
t ₄ f	1.2	1.2	0.8	1.4	1.5	0.6	2.0	1.7	0.6	t ₄ r	1.1	1.1	0.8	1.4	1.3	0.6	2.1	1.7	0.7
t ₅ f	0.6	0.8	0.8	0.9	1.1	0.7	1.4	1.4	0.8	t ₅ r	1.1	1.0	0.8	0.7	0.7	0.4	2.3	1.8	0.8
t ₆ f	0.1	0.1	0.1	0.3	0.4	0.4	0.2	0.7	0.9	t ₆ r	0.7	0.6	0.4	1.4	1.6	0.9	0.5	0.9	0.8
t ₇ f	0.5	0.5	0.4	1.0	0.8	0.4	0.9	1.1	0.8	t ₇ r	0.1	0.1	0.1	0.7	0.8	0.6	1.0	1.1	1.0
t ₈ f	0.5	0.7	0.7	0.9	1.0	0.6	1.3	1.3	0.8	t ₈ r	0.3	1.3	1.9	0.9	1.4	1.3	1.5	1.6	1.0

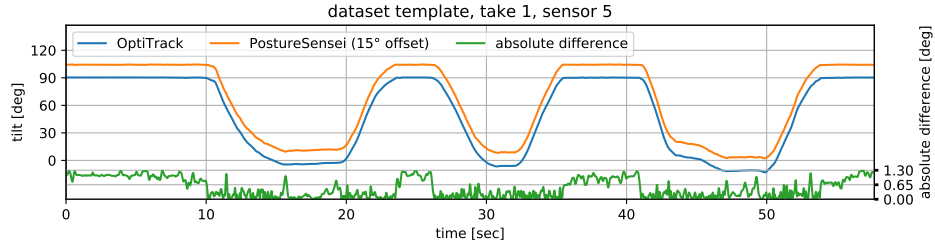


Figure 7. Tilt from tracking data (t_{opt} , blue), from accelerometer data (t_{acc} , orange, offset by 15°) and their absolute difference ($|t_{opt} - t_{acc}|$, green). For better readability we plotted only one sensor.

distances and standard deviations of the two resulting point clouds several times over different equally wide windows. Table 4 shows the resulting values. The spread of values for mean distances from 1 mm up to 8 mm with an average of $\mu = (3.4 \text{ mm} \pm 1.6 \text{ mm})$ are caused by the simplicity of the 2D spine curve model which does not incorporate factors such as skin deformation. We would like to point out that these values are obtained by comparing a set of 2D points embedded into 3D space with the native 3D coordinates of the motion capture system. The relatively small dispersion σ of usually less than 0.6 mm shows the consistency of the accelerometer data and that an even better spine curve representation can be reached by an improved model. Overall, these results show that the spine curve reconstruction is reproducible and usually highly similar to the OptiTrack recordings. This is also illustrated in Figure 8 where visually the different reconstructions show very similar shapes.

7 Limitations

Limitations of the robot arm: As discussed in Section 6.2 the robot arm rotation deviates substantially from the values programmed to the motor. The arm is connected to the motor by a rubber band to minimise transferred vibrations of the activated motor to the arm. The rubber band might slip when the motor is activated, and amplify swinging after stopping the rotation. Thus, we have to rely on the motion capture data. Additionally, the assumption of a rigid

Table 4. Dataset human posture, raw data. Mean and standard deviation (μ , σ) of the Euclidean distance between two aligned spine curves per 2D/3D sensor/marker position. $s_{i,j}$ abbreviates sensor/marker j in segment i . Values are measured in mm.

	$s_{1,1}$	$s_{1,2}$	$s_{1,3}$	$s_{1,4}$	$s_{1,5}$	$s_{2,1}$	$s_{2,2}$	$s_{2,3}$	$s_{2,4}$	$s_{2,5}$	$s_{3,1}$	$s_{3,2}$	$s_{3,3}$	$s_{3,4}$	$s_{3,5}$	$s_{4,1}$	$s_{4,2}$	$s_{4,3}$	$s_{4,4}$	$s_{4,5}$
μ	1.9	1.7	2.4	1.4	2.1	2.8	2.8	2.5	6.8	6.1	2.9	2.7	1.8	1.6	2.3	4.4	3.8	4.3	1.0	3.1
σ	0.3	0.2	0.3	0.3	0.5	0.3	0.1	0.7	0.8	1.1	0.5	0.5	0.6	0.6	0.8	0.3	0.3	0.4	0.4	0.5

	$s_{5,1}$	$s_{5,2}$	$s_{5,3}$	$s_{5,3}$	$s_{5,5}$	$s_{6,1}$	$s_{6,2}$	$s_{6,3}$	$s_{6,4}$	$s_{6,5}$	$s_{7,1}$	$s_{7,2}$	$s_{7,3}$	$s_{7,4}$	$s_{7,5}$	$s_{8,1}$	$s_{8,2}$	$s_{8,3}$	$s_{8,4}$	$s_{8,5}$
μ	3.4	3.4	1.8	1.8	2.6	4.9	3.8	3.8	1.2	3.5	4.7	4.6	2.8	2.8	3.3	7.6	6.9	5.6	2.7	5.4
σ	0.6	0.5	0.6	0.7	0.9	0.5	0.5	0.4	0.4	0.4	0.3	0.3	0.3	0.3	0.5	0.3	0.3	0.4	0.8	0.5

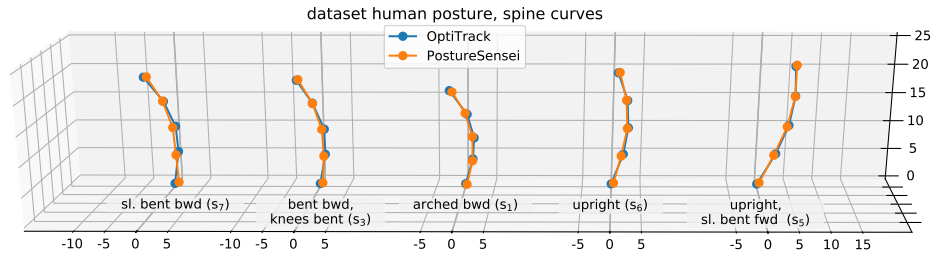


Figure 8. Aligned computed spine curves of various segments (orange lines) and 3D positions of the sensors from OptiTrack (blue lines).

body is not entirely realistic as we observe a slight bending ($< 2^\circ$) of the robot arm due to gravity.

Limitations of the sensor system: The *PostureSensei*TM system only measures accelerations. Thus, the estimation of the tilt angles only works well if relatively static poses are considered. Otherwise, accelerations in any other direction than gravity will influence the tilt computation and thus have an impact on the displayed spine curves. However, for slow motions, like we measured on the robot and on the template, tilt estimation worked well. More advanced sensors, including magnetic field sensors or gyroscopes could be used to capture reliable posture readings from dynamic motions.

Limitations of the pose reconstruction: Although the presented model for pose reconstruction is simple, it yields very good results for the human posture data. An extended model could expand to 3D reconstruction and integrate the flexibility in the human skin to even better approximate the actual shape and further reduce the reconstruction error along the spine curve.

8 Conclusion and Future Work

In this paper, we reported on a series of experiments to evaluate if an accelerometer-based wearable system can be used to accurately record the lumbar spine. As baseline for the experiments we recorded data from both systems simultaneously. Our main findings are:

1. Sensor tilt values can be captured with a very high precision ($0.4^\circ \pm 0.8^\circ$ for a single sensor), compared against motion capture data.
2. The computation of positional data works well (3.4 mm average deviation on a curve of 30 cm length), despite the simplistic model employed.
3. The visual spine representation is meaningful for postural feedback.

Thus, we conclude, that *PostureSensei*TM is capable of capturing the spinal curvature for static poses accurately and provides valuable feedback to the user.

We are planning to do user studies on the effectiveness of wearable devices in posture training in the future. Another interesting strand of research will be to explore how far the accuracy of pose reconstruction can be improved by a more advanced spine reconstruction model as well as adding more sensor modalities, such as magnetic field or gyroscopes to the wearable sensor units.

Acknowledgement. We thank Philipp Löschner and David Scherfgen for supporting us with the motion capture recordings.

References

1. Robertson, J.T.: The rape of the spine. *Surgical Neurology* **39**(1) (1993) 5 – 12
2. Vällfors, B.: Acute, subacute and chronic low back pain: clinical symptoms, absenteeism and working environment. *Scandinavian journal of rehabilitation medicine. Supplement* **11** (1985) 198
3. Rubin, D.I.: Epidemiology and risk factors for spine pain. *Neurologic Clinics* **25**(2) (2007) 353 – 371 Neck and Back Pain.
4. Gaskin, D.J., Richard, P.: The economic costs of pain in the united states. *The Journal of Pain* **13**(8) (2012) 715–724
5. Peleg, M., Leung, T.I., Desai, M., Dumontier, M. In: *Is Crowdsourcing Patient-Reported Outcomes the Future of Evidence-Based Medicine? A Case Study of Back Pain*. Springer International Publishing, Cham (2017) 245–255
6. Colombo, S., Joy, M., Mason, L., Peper, E., Harvey, R., Booiman, A.: Posture change feedback training and its effect on health. In: *48th Annual Meeting of the Association for Applied Psychophysiology and Biofeedback*. (March 2017)
7. Hellstrom, P.A.R., Åkerberg, A., Folke, M.: Posture sensor as feedback when lifting weights. In: *4th International Conference on Ambulatory Monitoring of Physical Activity and Movement*. (June 2015)
8. Fathi, A., Curran, K.: Detection of spine curvature using wireless sensors. *Journal of King Saud University-Science* **29**(4) (2017) 553–560
9. Noiunkar, S., Tirakoat, S.: Use of optical motion capture in sports science: A case study of golf swing. In: *Informatics and Creative Multimedia (ICICM), 2013 International Conference on, IEEE* (2013) 310–313
10. MacIver, M., Sharabash, N., Nelson, M.: Prey-capture behavior in gymnotid electric fish: motion analysis and effects of water conductivity. *Journal of Experimental Biology* **204**(3) (2001) 543–557
11. Culhane, K.M., OConnor, M., Lyons, D., Lyons, G.M.: Accelerometers in rehabilitation medicine for older adults. *Age and Ageing* **34**(6) (2005) 556–560
12. Merriaux, P., Dupuis, Y., Boutteau, R., Vasseur, P., Savatier, X.: A study of vicon system positioning performance. *Sensors* **17**(7) (2017)
13. Bernard, J., Dobermann, E., Vögele, A., Krüger, B., Kohlhammer, J., Fellner, D.: Visual-interactive semi-supervised labeling of human motion capture data. In: *Visualization and Data Analysis (VDA 2017)*. (January 2017)
14. Chen, X., Koskela, M.: Skeleton-based action recognition with extreme learning machines. *Neurocomputing* **149** (2015) 387–396
15. Wilhelm, N., Vögele, A., Zsoldos, R., Licka, T., Krüger, B., Bernard, J.: Furyexplorer: Visual-interactive exploration of horse motion capture data. In: *Visualization and Data Analysis (VDA 2015)*. (February 2015)
16. Zsoldos, R., Krüger, B., Licka, T.: From maturity to old age: tasks of daily life require a different muscle use in horses. *Comparative Exercise Physiology* **10**(2) (July 2014) 75–88
17. Müller, M., Röder, T., Clausen, M., Eberhardt, B., Krüger, B., Weber, A.: Documentation mocap database hdm05. Technical Report CG-2007-2, Universität Bonn (June 2007)
18. CMU: Carnegie Mellon University Graphics Lab: Motion Capture Database (2013)

19. Riaz, Q., Krüger, B., Weber, A.: A relational database for human motion data. *Lecture Notes in Computer Science, Computational Science and Its Applications - ICCSA 2015* **9159** (June 2015) 234–249
20. Kapadia, M., Chiang, I.k., Thomas, T., Badler, N.I., Kider Jr, J.T., et al.: Efficient motion retrieval in large motion databases. In: *Proceedings of the ACM SIGGRAPH Symposium on Interactive 3D Graphics and Games, ACM* (2013) 19–28
21. Wang, P., Lau, R.W., Zhang, M., Wang, J., Song, H., Pan, Z.: A real-time database architecture for motion capture data. In: *Proceedings of the 19th ACM international conference on Multimedia, ACM* (2011) 1337–1340
22. Awad, C., Courty, N., Gibet, S.: A database architecture for real-time motion retrieval. In: *Content-Based Multimedia Indexing, 2009. CBMI'09. Seventh International Workshop on, IEEE* (2009) 225–230
23. Pavlakos, G., Zhou, X., Derpanis, K.G., Daniilidis, K.: Coarse-to-fine volumetric prediction for single-image 3d human pose. In: *Computer Vision and Pattern Recognition (CVPR), 2017 IEEE Conference on, IEEE* (2017) 1263–1272
24. Bogo, F., Kanazawa, A., Lassner, C., Gehler, P., Romero, J., Black, M.J.: Keep it simple: Automatic estimation of 3d human pose and shape from a single image. In: *European Conference on Computer Vision, Springer* (2016) 561–578
25. Rhodin, H., Richardt, C., Casas, D., Insafutdinov, E., Shafiei, M., Seidel, H.P., Schiele, B., Theobalt, C.: Egocap: egocentric marker-less motion capture with two fisheye cameras. *ACM Transactions on Graphics (TOG)* **35**(6) (2016) 162
26. Shiratori, T., Park, H.S., Sigal, L., Sheikh, Y., Hodgins, J.K.: Motion capture from body-mounted cameras. *ACM Trans. Graph.* **30**(4) (July 2011) 31:1–31:10
27. Vögele, A., Zsoldos, R., Krüger, B., Licka, T.: Novel methods for surface emg analysis and exploration based on multi-modal gaussian mixture models. *PLOS ONE* (June 2016)
28. Weiss, A., Herman, T., Plotnik, M., Brozgol, M., Maidan, I., Giladi, N., Gurevich, T., Hausdorff, J.M.: Can an accelerometer enhance the utility of the timed up & go test when evaluating patients with parkinson's disease? *Medical Engineering & Physics* **32**(2) (2010) 119 – 125
29. Bourke, A., O'Brien, J., Lyons, G.: Evaluation of a threshold-based tri-axial accelerometer fall detection algorithm. *Gait & Posture* **26**(2) (2007) 194 – 199
30. Riaz, Q., Guan hong, T., Krüger, B., Weber, A.: Motion reconstruction using very few accelerometers and ground contacts. *Graphical Models* (April 2015)
31. Slyper, R., Hodgins, J.K.: Action capture with accelerometers. In: *Proceedings of the 2008 ACM SIGGRAPH/Eurographics Symposium on Computer Animation. SCA '08, Eurographics Association* (2008) 193–199
32. Vlastic, D., Adelsberger, R., Vannucci, G., Barnwell, J., Gross, M., Matusik, W., Popović, J.: Practical motion capture in everyday surroundings. *ACM Trans. Graph.* **26**(3) (July 2007)
33. Farella, E., Benini, L., Riccò, B., Acquaviva, A.: Moca: A low-power, low-cost motion capture system based on integrated accelerometers. *Adv. MultiMedia* **2007**(1) (January 2007) 1–1
34. Riaz, Q., Vögele, A., Krüger, B., Weber, A.: One small step for a man: Estimation of gender, age, and height from recordings of one step by a single inertial sensor. *Sensors* **15**(12) (December 2015) 31999–32019
35. Gower, J.C., Dijksterhuis, G.B.: Procrustes problems. Volume 30 of *Oxford Statistical Science Series*. Oxford University Press, Oxford, UK (January 2004)